

5 Surface/Interface Magnetism Project

– Crystalline, magnetic and electronic structures at the surface and interface of magnetic thin films and multilayers –

Project Leader: Kenta Amemiya

5-1 Introduction

The surface and interface of magnetic thin films play essential roles in the appearance of extraordinary magnetic properties such as perpendicular magnetic anisotropy (PMA) and the giant magnetoresistance effect. We are investigating the crystalline, magnetic and electronic structures at the surface and interface of magnetic thin films and multilayers, in order to reveal the origin of fascinating magnetic properties that cannot be realized in bulk materials. For example, we have studied magnetic anisotropy of Fe/Ni multilayers [1-4], magnetic structures at the interface between antiferromagnetic FeMn and ferromagnetic Ni [5,6], effects of ion irradiation on magnetism of ultrathin films [7,8], and a voltage-induced change in magnetic behavior of Fe and FeCo thin films grown on a ferroelectric substrate [9,10], by means of X-ray magnetic circular dichroism (XMCD), extended X-ray absorption fine structure (EXAFS), and polarized neutron reflectivity (PNR) techniques. We also plan to perform muon spin rotation experiments using an ultra-slow muon source.

5-2 Scientific topics 1: Anomalous magnetic structure at the interface between ferromagnetic Ni and antiferromagnetic FeMn [5,6]

The magnetic anisotropy interaction between antiferromagnetic (AFM) and ferromagnetic (FM) materials has been extensively investigated [5,11,12]. It was reported that the magnetic easy axis of ~10 monolayer (ML) Ni films switches from the perpendicular to in-plane directions when the films are attached to an AFM FeMn film [11], which indicates that the AFM FeMn film

enhances in-plane magnetic anisotropy. The change in magnetic anisotropy induced by AFM FeMn is explained by the magnetic frustration between Ni and FeMn, i.e., since each atomic layer in FeMn has net perpendicular magnetization which is opposite to that in the adjacent layer, the magnetic moment in perpendicularly magnetized Ni undergoes a frustration at the FeMn/Ni interface if the interface has atomic-layer steps. Recently, we have suggested a twisted magnetic structure, in which the Ni magnetic moment is rotated from the perpendicular to in-plane directions towards the interface with AFM FeMn [5], by means of complementary use of depth-resolved XMCD [13,14] and PNR techniques. In this report, we discuss the in-plane magnetic field dependence of the canted magnetic moment around the interface between AFM FeMn and FM Ni.

To obtain depth-resolved information on the magnetic moment in Ni under different magnetic fields, a PNR experiment was carried out at BL-17 (SHARAKU) in the Materials and Life Science Experimental Facility, Japan Proton Accelerator Research Complex, using a pulsed neutron source [15]. Magnetic fields, H , of up to 10 kOe were applied along the film plane, and the neutron polarization was also in the film plane. Specular reflectivity curves, R^+ and R^- , were measured using a ^3He single neutron detector at glancing angles of 0.3, 0.9, and 2.7 deg to cover a wide wave number (q) range. Here, R^+ and R^- represent the reflectivity when the neutron polarization is parallel and antiparallel to the magnetic field at the sample position, respectively, which were measured without a spin analyzer. The PNR measurement was performed at room temperature. A Cu/FeMn/Ni/Cu(100) film, which exhibits perpendicular magnetization in the remanent state, was investigated.

Figure 1 shows PNR curves for Cu/FeMn/Ni/Cu(100) taken at different in-plane magnetic fields, H . The Cu, FeMn and Ni layer thicknesses were ~ 70 , ~ 20 , and ~ 11 ML, respectively. Since the film shows perpendicular magnetization in the remanent state, the PNR data reflects the in-plane component of the magnetic moment induced by the magnetic field. In fact, the difference between R^+ and R^- is undetectable at $H = 0$ kOe, and it gradually increases with increasing H . Then the observed PNR curves are fitted by using a two-region model, in which the Ni film is separated into two regions, the interface and inner part of the film, which have different in-plane magnetic moments. Since the net in-plane magnetic moment in each atomic layer of FeMn vanishes due to the AFM coupling, the magnetic structure of FeMn was not considered in the fitting procedure. We optimized the magnetic moments in the interface and inner regions for each H , while the other parameters, scattering length density (SLD), film thickness, and roughness, were assumed to be the same for all H . To emphasize the magnetic contribution in the PNR curve, $\Delta R/R_{av}$ is plotted in Fig. 2, together with the fitting result. Here, $\Delta R = R^+ - R^-$, and R_{av} represents the average between R^+ and R^- . The overall shape of $\Delta R/R_{av}$ is basically the same for

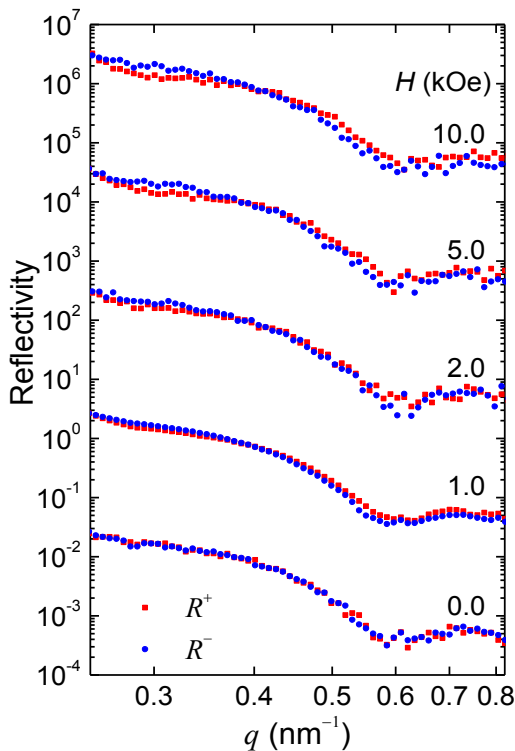


Fig. 1: PNR curves, R^+ and R^- , for Cu/FeMn/Ni/Cu(100) measured at different magnetic fields, H . The data for different H are vertically shifted.

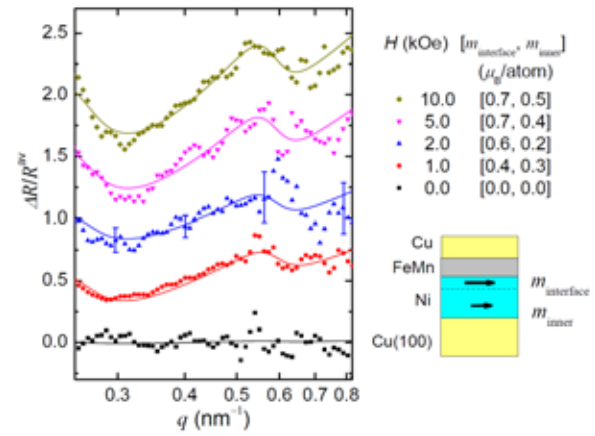


Fig. 2: Difference in the PNR curves, $\Delta R = R^+ - R^-$, divided by the average of them, $R_{av} = (R^+ + R^-)/2$, for Cu/FeMn/Ni/Cu(100) measured at different magnetic fields, H . The data for different H are vertically shifted. The lines are the simulated curves using the in-plane magnetic moments in the interface and inner regions of the Ni film, $m_{interface}$ and m_{inner} , respectively, indicated in the figure.

all H , but one can recognize that the magnetic field dependence cannot be explained by just multiplying scaling factors to the $\Delta R/R_{av}$ curves.

The obtained results are interpreted as follows, with the help of the depth-resolved XMCD results [5]. The Ni L-edge depth-resolved XMCD reveals that, in the case of a film with the Ni thickness of 16 ML which shows perpendicular magnetization in the remanent state, the perpendicular magnetic component in Ni decreases as the probing depth decreases, i.e., as the surface sensitivity increases. On the other hand, in the case of 7.5 ML Ni which shows in-plane magnetization in the remanent state, the in-plane magnetic moment does not decrease but is almost constant independent of the probing depth. By combining these results with those obtained by PNR, it is suggested that the magnetic moment in Ni prefers the in-plane direction around the interface with FeMn. Therefore, a twisted magnetic structure is expected to be realized when a weak in-plane magnetic field is applied to an FeMn/Ni film which shows perpendicular magnetization in the remanent state. Here, it may seem strange that the perpendicular component around the interface with FeMn decreases in the remanent state, $H = 0$ kOe, while no in-plane magnetic moment is observed by PNR. However, it can be interpreted by the formation of the domain structure, in which the in-plane magnetic components cancel each other out.

Figure 3 shows the magnetic field (H) dependence of the in-plane components of the

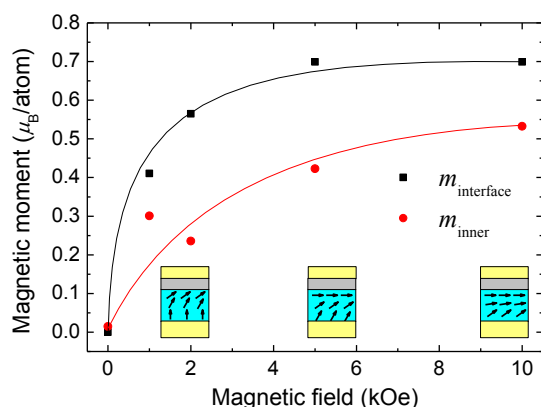


Fig. 3: In-plane component of the magnetic moment in the interface and inner region of the Ni film, estimated by fitting the PNR curves, as a function of applied magnetic field, H . The lines are guides for the eye. The expected magnetic structure is schematically illustrated.

magnetic moment in the interface and inner regions of the Ni film obtained from the PNR analysis. It is revealed that the magnetic moment around the interface with FeMn rapidly rotates to the in-plane direction with increasing H , which leads to the twisted magnetic structure as discussed above. At higher H , the magnetic moment in the inner region also aligns in the in-plane direction as illustrated in Fig. 3. It is thus suggested that the anomalous magnetic behavior is due to the magnetic anisotropy interaction between the AFM FeMn and FM Ni.

5-3 Scientific topics 2: Voltage-induced changes in magnetization and structure of Fe thin films grown on BaTiO₃

One of the most usual ways to control the direction of the spin moment in a magnetic material is to apply a magnetic field generated by an electromagnet. It requires a relatively large current to generate a magnetic field. On the other hand, it has been shown that the spin direction can be switched by a spin polarized current, in which a much smaller current is required compared with the switching by a magnetic field, especially in the case of nanometer-scale magnets such as those in a magnetic recording device. Moreover, electric field-induced magnetization switching was recently demonstrated [16], which has great potential to reduce the energy consumption in the magnetization switching process.

The idea of controlling magnetization by an electric field has been proposed as the “multiferroic”

concept [17]. For instance, BiFeO₃ has been extensively investigated as one of the most promising multiferroic materials. Unfortunately, the temperature at which such materials show the multiferroic property is usually far below room temperature in the case of single compound materials. On the other hand, it was reported that the coercive field of a ferromagnetic Fe thin film grown on a ferroelectric BaTiO₃ (BTO) substrate changes when a voltage is applied between the Fe film and the bottom of the substrate, even at room temperature [18]. Since the mechanism of the voltage-induced effects on the magnetic properties has not been clearly understood, we have performed XMCD and EXAFS measurements for Fe thin films grown on the BTO substrate, and observed the change in the interface state induced by electric polarization reversal of the substrate. Fe L-edge XMCD spectra were taken at the soft X-ray undulator beamline BL-16A of the Photon Factory (PF) [19], and the Fe K-edge EXAFS spectra were measured at the bending magnet beamline BL-12C of the PF.

Figure 4 displays the XMCD-hysteresis curves measured at the Fe L₃ absorption edge (707.5 eV) of an 8 nm Fe thin film grown on the BTO substrate at different electric fields, E . All the curves show small squareness ratio, which indicates that the Fe film shows weak in-plane magnetic anisotropy. Under such magnetic conditions, the magnetic domain structure of Fe could be influenced by the ferroelectric domain structure of the BTO substrate.

Figure 5 shows the electric field dependence of the residual magnetization, M_0 (a), and the coercive field, H_c (b). The electric field is changed from $E = 10$ kV/cm, as indicated by the arrows in the figure. Both M_0 and H_c show the maximum at $\sim \pm 3$ kV/cm, and a hysteresis behavior is observed. Indeed, it is known that the ferroelectric domain of BTO under the tetragonal phase shows a multi-domain structure after going through the zero-field during the polarization reversal. We assume that the coercive field of Fe increases because of the multi-domain formation, which obstructs the movement of the magnetic domains.

Figure 6 displays the XMCD spectra of the 8 nm Fe film on the BTO substrate. No significant difference by the electric polarization reversal is observed in the spectra. This result indicates that the change in M_0 and H_c by the electric polarization reversal is not caused by the change in the electronic state of Fe itself, but by the ferroelectric

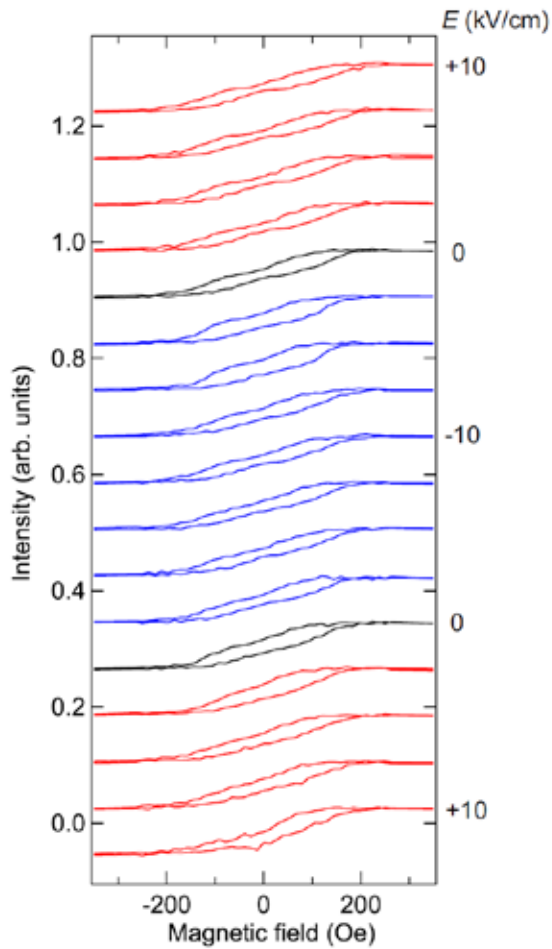


Fig. 4: XMCD-hysteresis curves measured at Fe L_3 absorption edge of 8 nm Fe thin film on the BTO substrate at different electric fields, E .

domain structure of the BTO substrate. Because the domain structure of BTO is expected to affect the crystal structure of Fe film, we apply Fe K-edge EXAFS structural analysis to the film.

Figure 7 shows Fourier transforms of the Fe K-edge EXAFS function $k^2(k)$ of the 8 nm Fe film on the BTO substrate. For all the spectra, a large peak at a distance of ~ 1.6 Å is observed, which corresponds to the Fe–O bond. Moreover, other peaks appear at ~ 2.0 and 2.5 Å, and they come from the Fe–Fe scattering. This suggests that there exists an Fe oxide other than the Fe metal phase, and it could be formed by the hybridization between Fe and BTO at the interface.

We further analyze the EXAFS data in order to obtain quantitative structural parameters. Figure 8 shows the deviation of the in-plane bond distances for Fe–O (a) and Fe–Fe (b), as a function of the electric field, E . Note that the electric field is changed from $E = -10$ kV/cm, as indicated by the arrows in the figure, and the deviation is estimated by setting the first point as a standard. The rate of

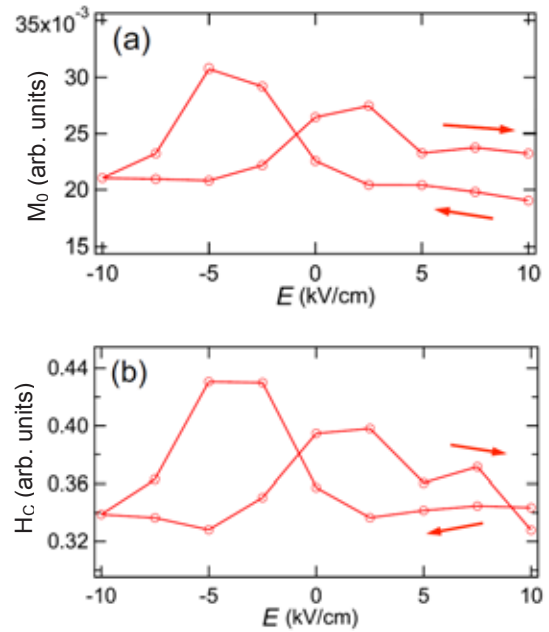


Fig. 5: Electric field dependence of the residual magnetization, M_0 (a), and the coercive field, H_c (b). The electric field is changed from 10 kV/cm, as indicated by the arrows.

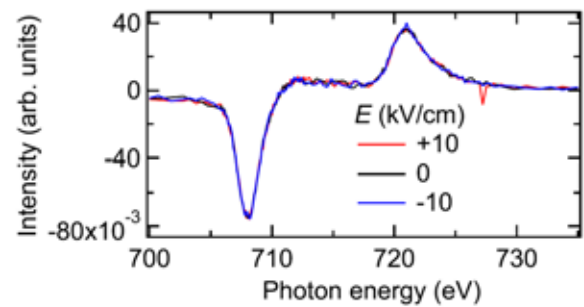


Fig. 6: XMCD spectra of 8 nm Fe film on the BTO substrate measured at the electric field of +10, 0 and -10 kV/cm.

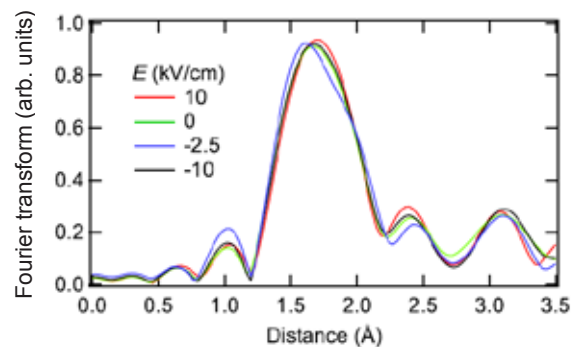


Fig. 7: Fourier transforms of the Fe K-edge EXAFS function $k^2(k)$ of 8 nm Fe film on the BTO substrate.

change of the distance with respect to the electric field is larger for the Fe–O bond compared to the Fe–Fe one. This means that the local structure

of the interfacial Fe oxide can be easily affected by the ferroelectric domain structure of the BTO substrate. Furthermore, the response to the electric field is very similar to that of M_0 and H_c as shown in Fig. 5. That is, the in-plane bond distance for Fe-O shows a hysteresis behavior, and shows a shorter distance at $\sim \pm 3$ kV/cm. These results indicate that the in-plane Fe-O distance is shorter when H_c is larger, in which the multi-domain structure in the BTO substrate is formed. On the other hand, the Fe-O distance is larger when H_c is smaller, in which BTO shows a single domain-like structure. In the former situation, the lateral connection of the Fe oxide over the grain boundary must be weak, and island-like localization is expected. We suppose that the localization of the interface Fe oxide leads to an enhancement of H_c of Fe.

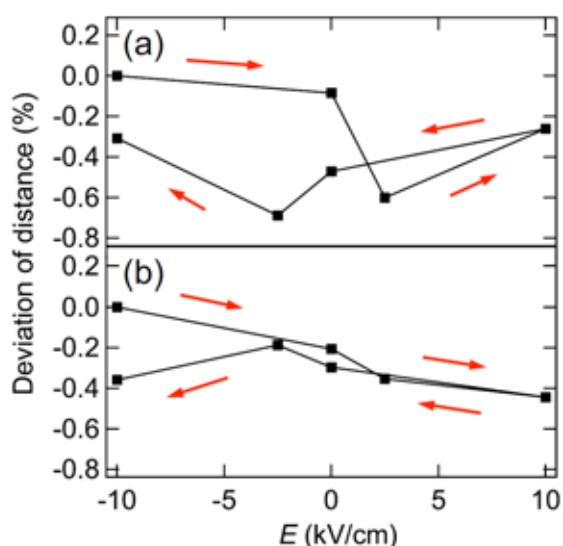


Fig. 8: Deviation of the in-plane bond distances for Fe-O (a) and Fe-Fe (b), as a function of the electric field, E . The electric field is changed from $E = -10$ kV/cm, as indicated by the arrows.

References

- [1] M. Sakamaki and K. Amemiya, *Appl. Phys. Express* **4** (2011) 073002.
- [2] M. Sakamaki and K. Amemiya, *e-J. Surf. Sci. Nanotech.* **10** (2012) 97.
- [3] M. Sakamaki and K. Amemiya, *Phys. Rev. B* **87** (2013) 014428.
- [4] M. Sakamaki and K. Amemiya, *J. Phys.: Cond. Matter* **26** (2014) 166002.
- [5] K. Amemiya et al., *Phys. Rev. B* **89** (2014) 054404.
- [6] K. Amemiya et al., *JPS Conf. Proc.*, in press.
- [7] M. Sakamaki et al., *Phys. Rev. B* **86** (2012) 024418.
- [8] K. Amemiya et al., *Eur. Phys. J. Web of Conf.* **40** (2013) 08002.
- [9] M. Sakamaki and K. Amemiya, *e-J. Surf. Sci. Nanotech.* **13** (2015) 139.
- [10] K. Amemiya and M. Sakamaki, submitted to *e-J. Surf. Sci. Nanotech.*
- [11] J. Wu et al., *Phys. Rev. B* **79** (2009) 212411.
- [12] H. C. Choi et al., *Phys. Rev. B* **81** (2010) 224410.
- [13] K. Amemiya, *Phys. Chem. Chem. Phys.* **14** (2012) 10477.
- [14] K. Amemiya et al., *Appl. Phys. Lett.* **84** (2004) 936.
- [15] M. Takeda et al., *Chin. J. Phys.* **50** (2012) 161.
- [16] Y. Shiota et al., *Nature Materials* **11** (2012) 39.
- [17] D. Khomskii, *Physics* **2** (2009) 20.
- [18] S. Brivio et al., *Appl. Phys. Lett.* **98** (2011) 092505.
- [19] K. Amemiya et al., *AIP Conf. Proc.* **1234** (2010) 295.

